



---

# **Project's report : Nerf optic sheath diameter measurement**

---

*Author :*

BADAOUI Abdennacer  
MRABET Hatim  
LITVIN Dmitri

*Supervisor :*

Ms. OUZIR Nora

# Table des matières

<b>1 Abstract</b>	<b>3</b>
<b>2 Introduction :</b>	<b>3</b>
<b>3 State of the art :</b>	<b>4</b>
<b>4 Dataset and preprocessing :</b>	<b>5</b>
<b>5 Metrics :</b>	<b>6</b>
5.1 Intersection over Union (IoU) . . . . .	6
5.2 Dice Coefficient . . . . .	7
5.3 Pixel Accuracy . . . . .	8
<b>6 Methodology :</b>	<b>8</b>
6.1 Feature extraction with VGG Model and segmentation with clustering algorithms . . . . .	9
6.1.1 Description of the model . . . . .	9
6.1.2 Results . . . . .	10
6.1.3 Conclusion . . . . .	12
6.2 Processing the images before training our model . . . . .	12
6.2.1 Description of the method . . . . .	12
6.2.2 Results . . . . .	13
6.2.3 Conclusion . . . . .	14
6.3 Segmentation with simple U-Net architecture . . . . .	15
6.4 Transfer learning . . . . .	17
6.4.1 Description of the method . . . . .	17
6.4.2 Results . . . . .	18
6.4.3 Performance evaluation and metrics . . . . .	20
6.4.4 Conclusion . . . . .	23
6.5 Alternative transfer learning approach . . . . .	24
6.5.1 Description of the method . . . . .	24
6.5.2 Results . . . . .	25
6.5.3 Performance evaluation and metrics . . . . .	27
6.5.4 Conclusion . . . . .	28
<b>7 Conclusion</b>	<b>29</b>
<b>8 Future Directions and Perspectives</b>	<b>29</b>

<b>9 Bibliography</b>	<b>30</b>
-----------------------	-----------

## 1 Abstract

This report presents a project focused on ultrasound image segmentation of the optic nerve sheath for measuring its diameter. The initial dataset consisted of 15 images, each accompanied by corresponding labels in the form of masks. The goal was to develop a model capable of accurately detecting these masks. Several methods were explored, starting with feature extraction using the VGG Model, followed by clustering algorithms. However, these approaches did not yield satisfactory results. Consequently, image processing techniques were incorporated prior to feature extraction and clustering algorithms, but their accuracy remained suboptimal.

To address the limitations, the project employed the Unet model, which was trained on the available dataset. Since the dataset was limited, the initial results were not highly accurate. To improve performance, data augmentation techniques such as flipping and rotating were applied, resulting in enhanced outcomes. Furthermore, transfer learning was utilized by training the encoder part of the Unet model on a large dataset for breast cancer detection, while the decoder parts were trained using the initial dataset. This transfer learning approach yielded even better results.

To further enhance the model's performance, an additional large dataset specific to optic nerve sheath images was incorporated, again employing transfer learning. This final step resulted in the best overall results achieved throughout the project. The primary challenges encountered during the project were primarily attributed to the limited availability of data, which adversely affected the performance of the models.

**Keywords :** ultrasound image segmentation, optic nerve sheath, diameter measurement, feature extraction, clustering algorithms, U-Net model, data augmentation, transfer learning.

## 2 Introduction :

The optic nerve sheath is a protective layer of tissue that surrounds the optic nerve. The diameter of the optic nerve sheath is an important indicator of intracranial pressure, which can be elevated in various medical conditions such as brain tumors, hydrocephalus, and traumatic brain injury. Currently, measuring the diameter of the optic nerve sheath requires invasive procedures such as lumbar puncture or intracranial pressure monitoring. However, recent advances in deep learning techniques have made it possible to develop non-invasive tools

for measuring the diameter of the optic nerve sheath from ultrasound images.

This technical report describes a project aimed at building an accurate model for measuring the diameter of the optic nerve sheath using deep learning techniques. The project uses a very limited dataset and develops a model that can segment ultrasound images and then use the clusters to measure the diameter of the optic nerve sheath. The ultimate goal of this project is to develop a non-invasive tool for measuring intracranial pressure that can save lives by allowing medical professionals to act quickly in urgent cases.

### **3 State of the art :**

Recent advancements in optic nerve segmentation using deep learning techniques have shown promising results in the field. Kristen M. Meiburger's research focused on the development of an automated method for measuring optic nerve diameter (OND) and optic nerve sheath diameter (ONSD) using a deep learning technique known as UNet with a ResNet50 encoder. Their study utilized a dataset consisting of 201 images from 50 patients and compared the automatically generated measurements with manual ones performed by an operator. The results demonstrated a mean error of  $0.07 \pm 0.34$  mm for OND and  $-0.07 \pm 0.67$  mm for ONSD, indicating the potential of the developed system in standardizing and reducing variability in OND and ONSD measurements.

In another study by Clement Dubost, ocular ultrasonography was utilized to estimate raised intracranial pressure in preeclampsia. Optic nerve sheath diameter (ONSD) measurements were compared between 26 preeclamptic patients and 25 healthy pregnant women. Two measurements were taken for each optic nerve in both the transverse and sagittal planes using a 7.5 MHz ultrasound linear probe. The study found significantly greater median ONSD values in preeclamptic patients compared to healthy pregnant women, suggesting the potential of ocular ultrasonography as a tool for assessing intracranial pressure in such cases.

Furthermore, Shengfeng Liu and Yi Wang conducted a review on deep learning architectures and their applications in ultrasound (US) image analysis. They highlighted the importance of developing advanced automatic US image analysis methods to enhance objectivity and accuracy in US diagnosis. Deep learning, with its remarkable capabilities, demonstrated substantial potential for various automatic US image analysis tasks, including classification, detection, and segmentation. The review provided an overview of popular deep learning

architectures and discussed their applications in US image analysis, while also addressing the challenges and future trends in this domain.

Collectively, these studies showcase the advancements made in optic nerve segmentation using deep learning techniques. The use of automated methods not only reduces manual evaluation variability but also holds the potential to improve the standardization and accuracy of optic nerve measurements, facilitating diagnosis and monitoring of various neurological conditions.

## 4 Dataset and preprocessing :

The dataset for this project consisted of several types of images, with the main ones being the original ultrasound images of the optic nerve (1,2,3). There were a total of 15 of these images, and each image had a corresponding clustered image where segmentation was done manually (4,5,6). These clustered images served as our labels for training the deep learning model. Additionally, for each original image, there were 5 corresponding images that represent the different masks that we needed to predict (7,8,9).

Due to the inherent noise in ultrasound images, it was very challenging to distinguish between the different parts of the optic nerve. Therefore, we applied several preprocessing steps to enhance the quality of the images and improve the accuracy of the model. Firstly, we resized all of the images to unify their shapes and make them compatible with the input requirements of the model.

Next, we applied several image enhancement techniques to improve the quality of the images. This included filtering to remove noise, normalization to ensure consistent brightness and contrast levels, and edge detection to enhance the edges of the optic nerve.

We also performed data augmentation to increase the size of our dataset and improve the robustness of the model. This involved randomly flipping and rotating the images, as well as applying other transformations such as cropping and scaling.

Finally, we split the dataset into training, validation, and test sets, ensuring that the images were randomly assigned to each set. This helped us to evaluate the performance of the model on unseen data and prevent overfitting.

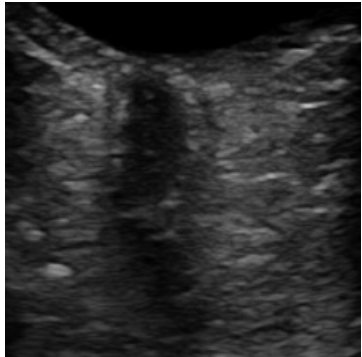


**FIGURE 1 –** Ultrasound image 1 of the optic nerve

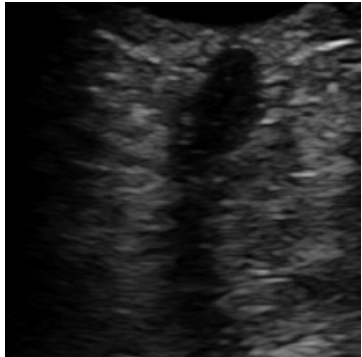


**FIGURE 2 –** Ultrasound image 2 of the optic nerve

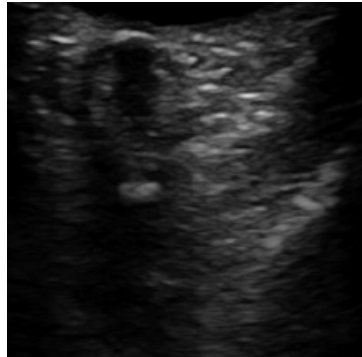


**FIGURE 3 –** Ultrasound image 3 of the optic nerve

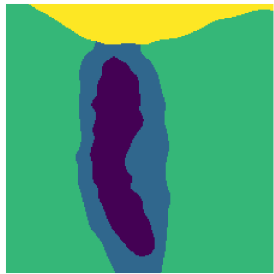


**FIGURE 4 –** Clustered image 1 of the optic nerve

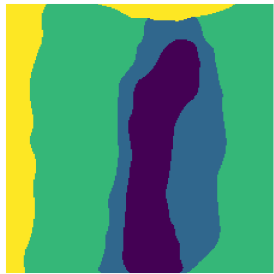


**FIGURE 5 –** Clustered image 2 of the optic nerve

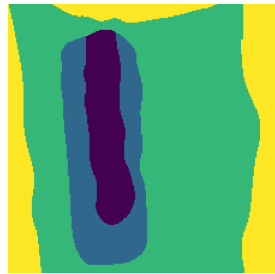


**FIGURE 6 –** Clustered image 3 of the optic nerve

## 5 Metrics :

In evaluating the performance of our segmentation model, we have chosen to utilize three key metrics : Intersection over Union (IoU), Dice Coefficient, and Pixel Accuracy.

### 5.1 *Intersection over Union (IoU)*

The Intersection over Union (IoU) metric provides an evaluation of the overlap between the true mask and the predicted mask. It quantifies how well

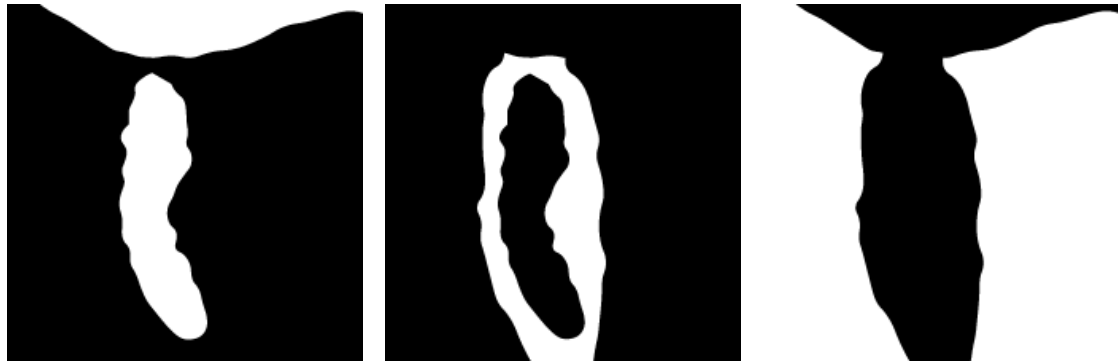


**FIGURE 7 –** Mask 1 of **FIGURE 8 –** Mask 2 of **FIGURE 9 –** Mask 3 of  
image 1 image 1 image 1

the model captures the common regions between the two masks. IoU is calculated by dividing the intersection of the masks by their union. A higher IoU score indicates a better segmentation accuracy, as it signifies a greater overlap between the predicted and true masks. This metric allows us to assess the spatial alignment and the extent to which the model accurately identifies the target regions. It's defined as follow :

$$IoU = \frac{\text{Area of overlap}}{\text{Area of union}}$$

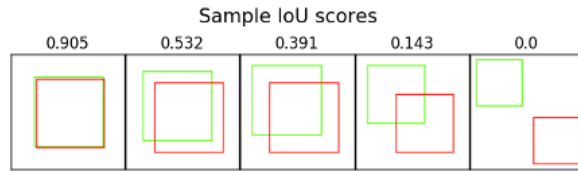


**FIGURE 10 –** IoU definition

## 5.2 Dice Coefficient

The Dice Coefficient is another widely used metric for segmentation evaluation. Similar to IoU, it measures the agreement between the true mask and the predicted mask. The Dice Coefficient considers both the presence and the shape similarity of the masks. It is calculated as twice the intersection of the masks divided by the sum of their areas. A higher Dice Coefficient implies a better segmentation performance, indicating a closer match between the predicted and true masks. This metric enables us to assess the model's ability to capture the target regions while considering their shapes and structures.

$$\text{Dice coefficient} = \frac{2 \times |A \cap B|}{|A| + |B|}$$

where :

- A represents the predicted segmentation mask or set
- B represents the ground truth segmentation mask or set
- $|A|$  represents the cardinality or size of set A
- $|B|$  represents the cardinality or size of set B
- $|A \cap B|$  represents the intersection or overlap between sets A and B, i.e., the number of common elements between the predicted and ground truth segmentation

### **5.3 Pixel Accuracy**

Pixel Accuracy is a fundamental metric that provides a general measure of overall accuracy in segmentation tasks. It calculates the percentage of correctly classified pixels in the predicted mask compared to the true mask. Pixel Accuracy focuses on the individual pixel level, providing an assessment of the model's ability to correctly classify each pixel. While it does not consider the spatial alignment or shape similarity, it offers a broad evaluation of the model's ability to accurately label pixels. This metric allows us to understand the overall performance of the segmentation model in terms of pixel-level accuracy. It's defined as follow :

$$\text{Pixel Accuracy} = \frac{\text{Number of correctly classified pixels}}{\text{Total number of pixels}}$$

By considering these three metrics - IoU, Dice Coefficient, and Pixel Accuracy - we gain a comprehensive evaluation of our segmentation model. Each metric provides valuable insights into different aspects of the model's performance, including spatial alignment, shape similarity, and pixel-level accuracy. This approach ensures a robust evaluation framework and enables us to assess the effectiveness of our segmentation approach for the specific problem domain.

## **6 Methodology :**

## 6.1 Feature extraction with VGG Model and segmentation with clustering algorithms

### 6.1.1 Description of the model

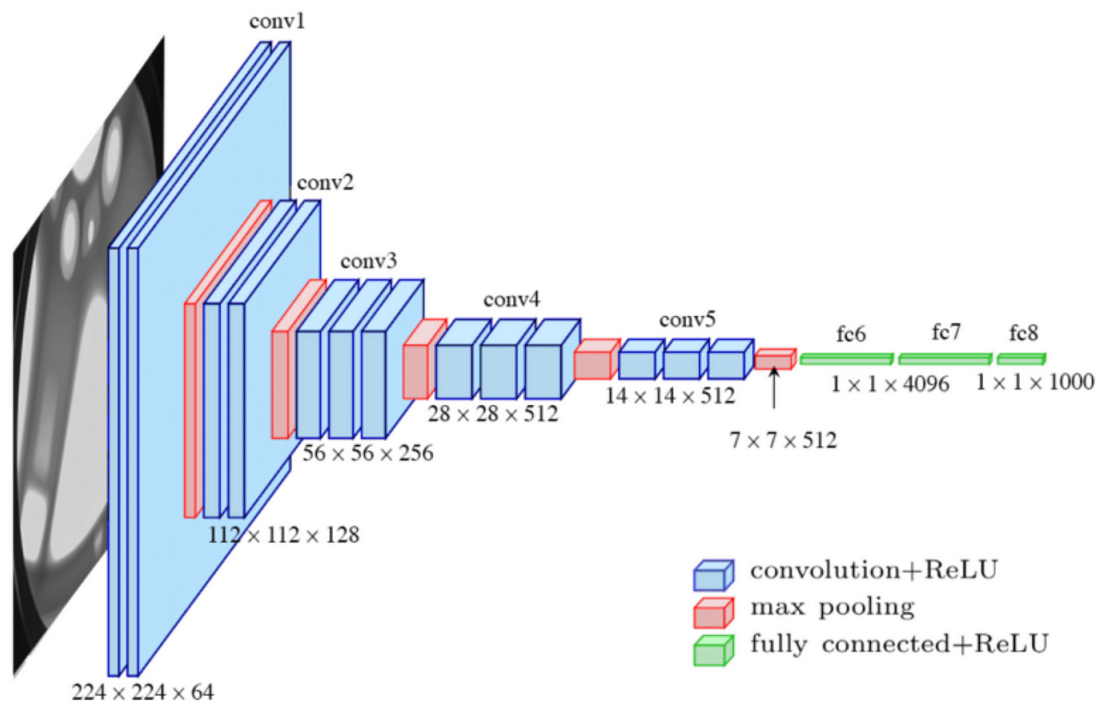


**FIGURE 11 – VGG16 model**

To effectively segment the image into different regions and generate distinct masks, we employed the use of the VGG model in conjunction with clustering algorithms. The VGG model, developed by the Visual Geometry Group at the University of Oxford, is a widely recognized convolutional neural network architecture known for its effectiveness in image classification and feature extraction tasks.

The VGG model offers a straightforward yet powerful approach to extract meaningful features from images. By employing a series of convolutional and pooling layers, the model captures both low-level and high-level features, allowing it to learn intricate patterns and representations present in the images. Its use of small receptive fields and deep stacking of convolutional layers enables the model to progressively learn more complex and discriminative features.

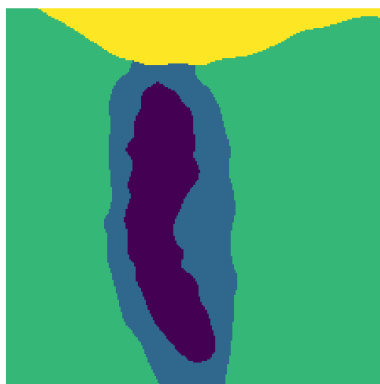
In our methodology, we utilized the VGG model as a feature extractor rather than for image classification purposes. We processed each pixel in the

image through the VGG model, obtaining a corresponding feature vector that encapsulates the extracted features. This step allowed us to capture both local and global information present in the image, enabling a richer representation of the image content.

Following the feature extraction step, we employed clustering algorithms to classify each pixel based on its feature vector. The primary objective was to group pixels with similar features together, forming distinct clusters that would correspond to different masks in the image. For classification, we used KMeans++ and DBSCAN.

### 6.1.2 Results

The results we obtained are exposed below :



**FIGURE 12 –** Ground truth result for image 1

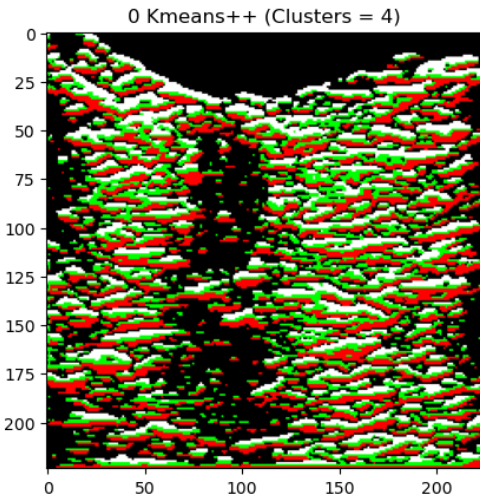


**FIGURE 13 –** Result for image 1

**FIGURE 14 –** Images



**FIGURE 15 –** Ground truth result for image 2

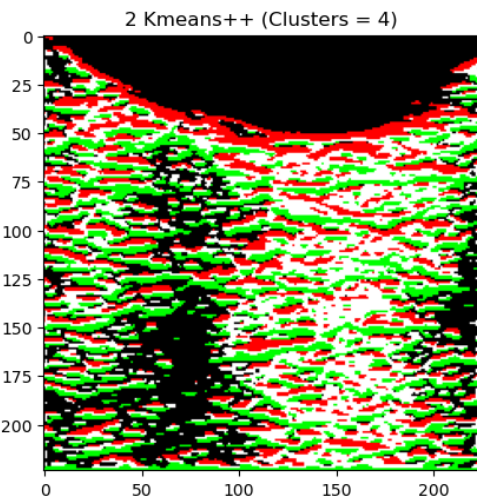


**FIGURE 16 –** Result for image 2

**FIGURE 17 –** Images

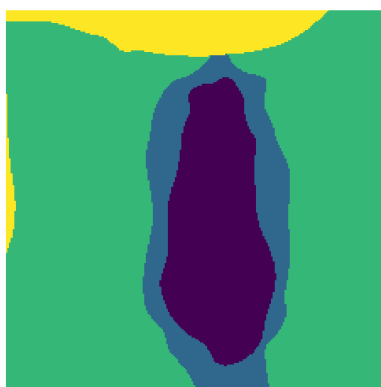


**FIGURE 18 –** Ground truth result for image 3

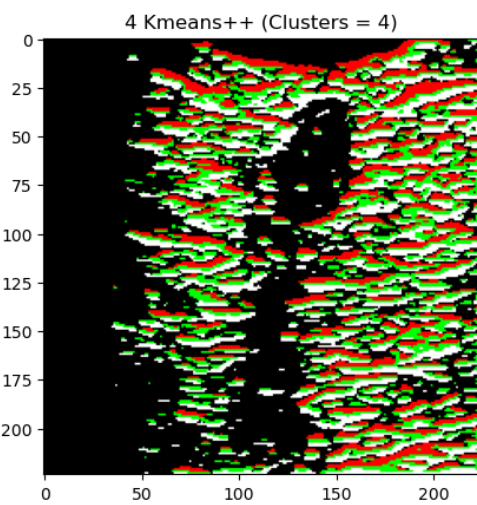


**FIGURE 19 –** Result for image 3

**FIGURE 20 –** Images

### 6.1.3 Conclusion

As we've seen through the metrics, this model was not very accurate, since it didn't allow to separate the different clusters, we notice that the image is still blurry and clusters were not well detected.

A first idea to move forward and develop our results is to make the images we want to segment clearer. As a consequence, we decided to apply some image processing techniques to our dataset, before training our model.

## 6.2 *Processing the images before training our model*

### 6.2.1 Description of the method

The contrast enhancement technique was employed as a pre-processing step. The primary objective of contrast enhancement was to improve the visual clarity and separability of clusters within the ultrasound images. By enhancing the contrast, the boundaries between different tissues or structures became more distinct and identifiable. This step facilitated better visualization of regions of interest and enabled more accurate identification of anatomical boundaries.

The advantages of contrast enhancement in ultrasound image segmentation are multi-fold. Firstly, it enhances the visibility of important features and textures within the images, allowing for more accurate feature extraction. Clearer and more distinguishable features contribute to improved segmentation accuracy. Secondly, by making clusters or regions of interest more separable, contrast enhancement reduces ambiguity and confusion between different regions, thereby enhancing segmentation accuracy.

Overall, the application of contrast enhancement significantly improved the quality of our results. We noticed that some clusters are being detected. Unfortunately, the results are still blurry, and we noticed that clusters still overlap, which means that our segmentation is still bad.

After the contrast enhancement, here are our new images :

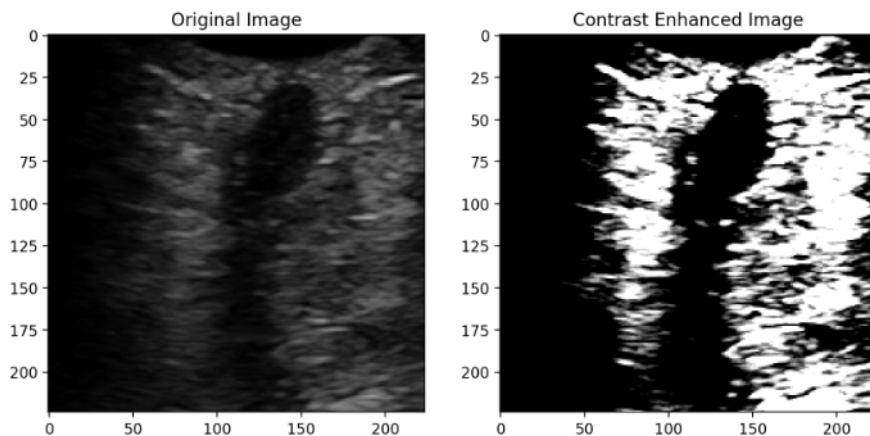


**FIGURE 21 –** Images with enhanced contrast

### 6.2.2 Results

Here are some results of this method :

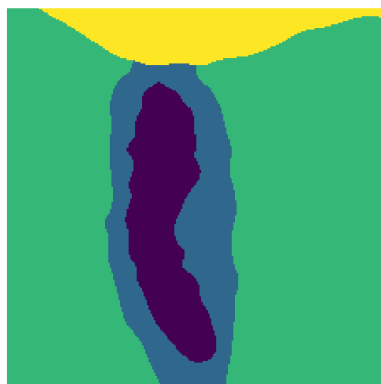


**FIGURE 22 –** Ground truth result for image 1

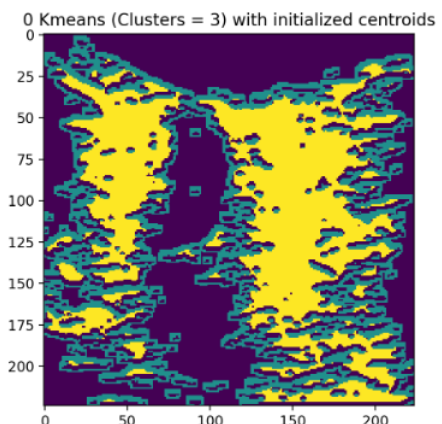


**FIGURE 23 –** Result for image 1

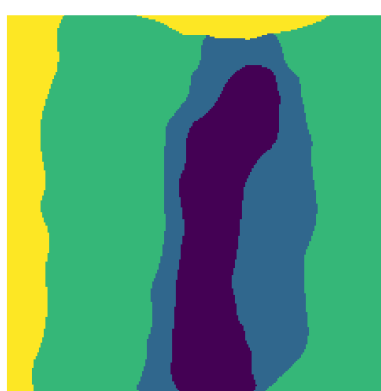


**FIGURE 24** – Ground truth result for image 2

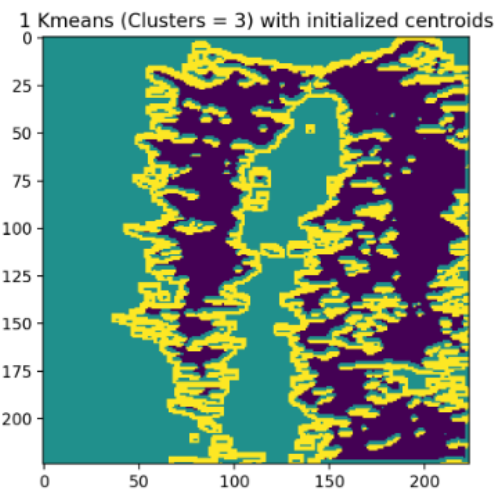


**FIGURE 25** – Result for image 2



**FIGURE 26** – Ground truth result for image 3

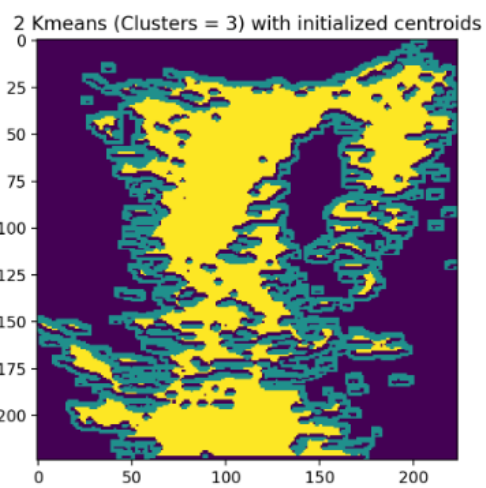


**FIGURE 27** – Result for image 3

### 6.2.3 Conclusion

- We noticed that this method didn't allow us to segment our images well, and the results are still blurry.
- At this point, maybe the methodology we followed was complex.

- We noticed that it's hard to differentiate the different clusters at once.
- Here comes a new idea of dealing with each cluster at once and making a model for each mask, instead of having one model that tries to find the three clusters at once.

### 6.3 Segmentation with simple U-Net architecture

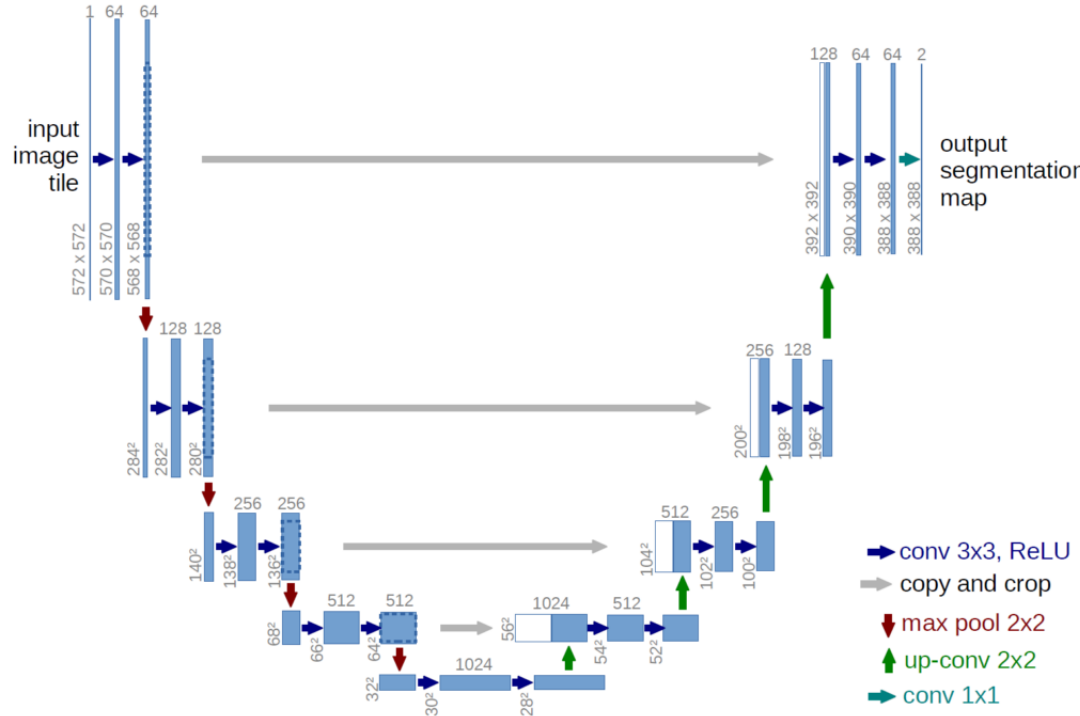
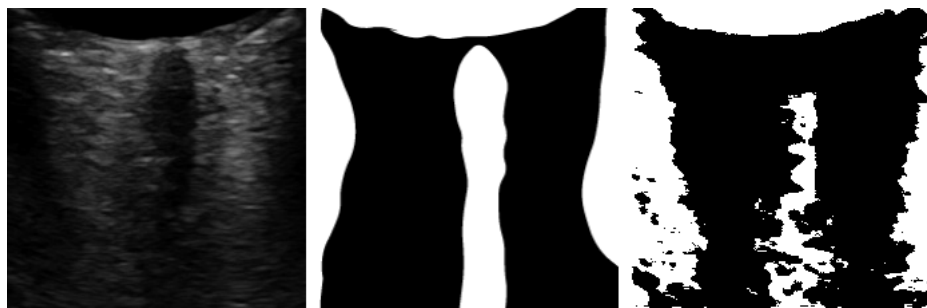


**FIGURE 28 – U-Net architecture**

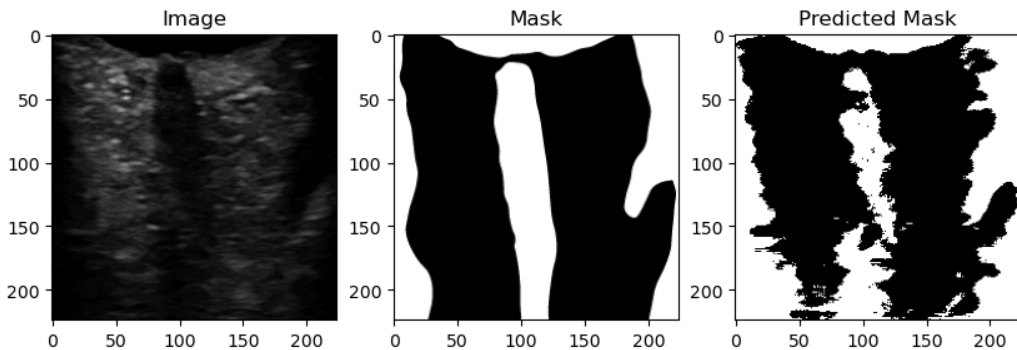
The choice of the U-Net architecture for segmenting ultrasound images of the optic nerve was driven by its effectiveness in accurately identifying and delineating specific regions within images. The U-Net architecture is specifically designed for image segmentation tasks, making it well-suited for the segmentation of the optic nerve in ultrasound images. Its encoder-decoder structure with skip connections allows for the extraction and integration of both local and global features, enabling precise segmentation results. By leveraging convolutional and transposed convolutional layers, the U-Net architecture effectively captures the intricate details and subtle boundaries of the optic nerve, contributing to the accuracy and reliability of the segmentation process. The utilization of U-Net in this project demonstrates a robust and state-of-the-art approach to optic nerve

segmentation, showcasing its potential for enhancing diagnostic and treatment capabilities in ophthalmology.

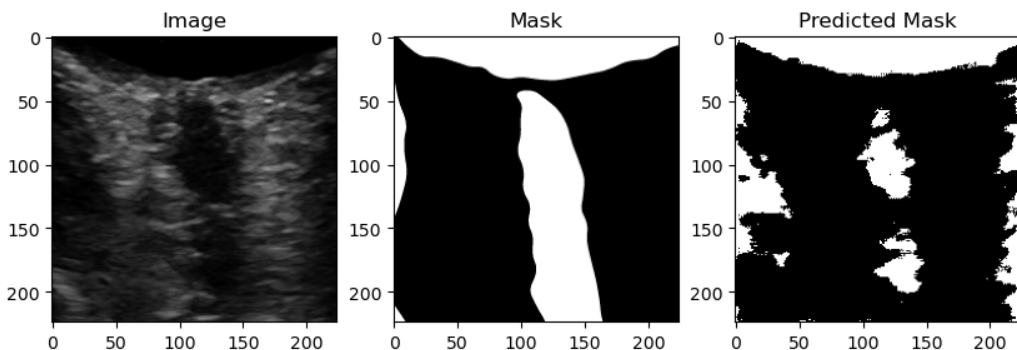
The following results were obtained using a UNet network with 3 encoders and 3 decoders. On the first mask, at first glance, the results seem to be correct, but not entirely correct. This is because it doesn't work for the other masks, especially mask 2. It appears that the model is simply trying to copy the real image and segment it independently of the shape of the mask.



**FIGURE 29 –** Image 1 of testset (Mask 1)



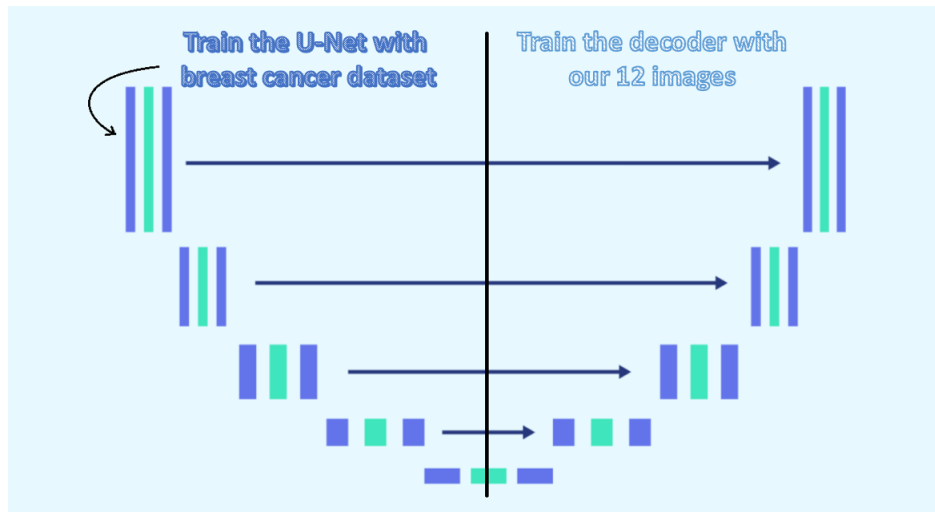
**FIGURE 30 –** Image 2 of testset (Mask 1)



**FIGURE 31 –** Image 3 of testset (Mask 1)

## 6.4 Transfer learning

### 6.4.1 Description of the method

**FIGURE 32 –** Unet Architecture with Transfer Learning

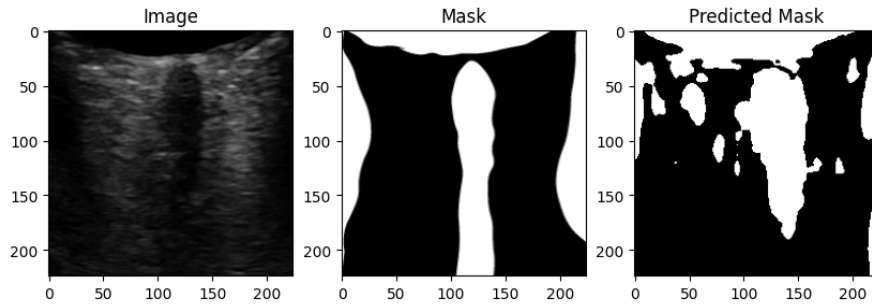
As we observed from the previous results, training a model on only 12 images may not be sufficient to achieve good performance. To overcome this limitation, we employed the technique of transfer learning. The basic idea behind transfer learning is to leverage knowledge gained from training a model on a large dataset, even if it is not directly related to the specific problem at hand.

In our approach, we adopted transfer learning by first training the encoder part of the previously used Unet architecture on a separate dataset of ultrasound images related to breast cancer. This initial training allowed the model to learn general features and patterns that are useful for various image segmentation tasks. By training on a larger and more diverse dataset, the model can capture more complex representations and gain better understanding of the underlying structures.

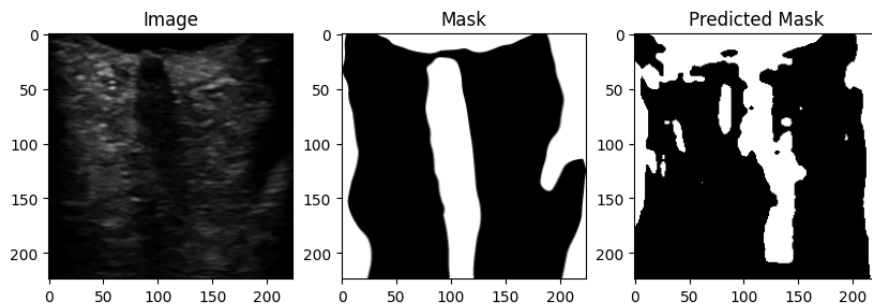
After training the encoder part of the Unet network, we created a new model that initialized the weights of the encoder with the pretrained weights. This new model had the same architecture as before, but only the decoder part needed further training. The decoder part was fine-tuned using our original dataset, which consisted of the 12 ultrasound images. By training the decoder part on our specific dataset, the model could adapt and learn to accurately segment the ultrasound images in the context of our problem.

#### 6.4.2 Results

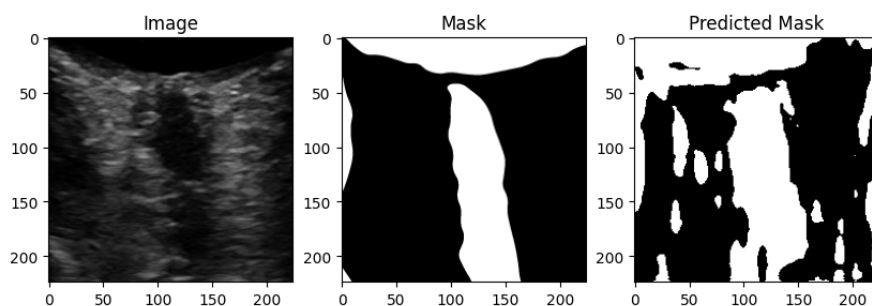
Here are the results obtained after applying the transfer learning technique :  
**Prediction of mask 1**



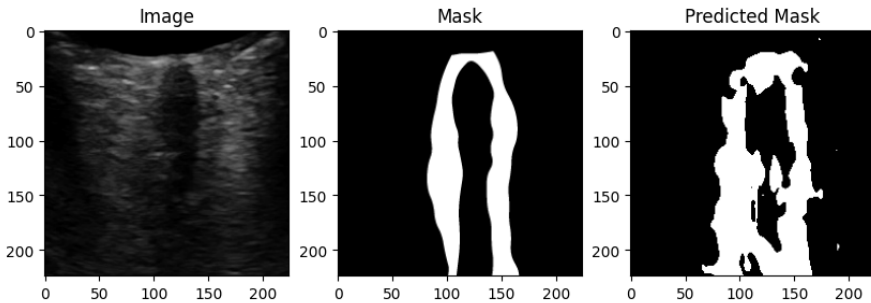
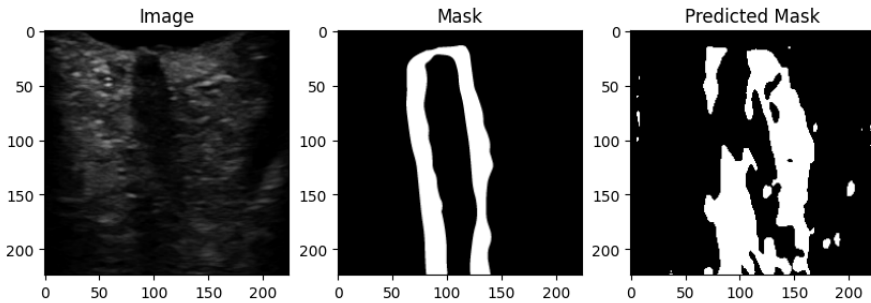
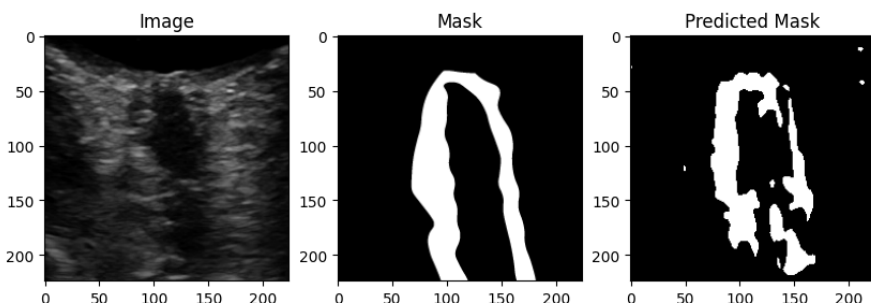
**FIGURE 33 –** Mask 1 of the first test image



**FIGURE 34 –** Mask 1 of the second test image



**FIGURE 35 –** Mask 1 of the third test image

**Prediction of mask 2****FIGURE 36 –** Mask 1 of the first test image**FIGURE 37 –** Mask 2 of the second test image**FIGURE 38 –** Mask 2 of the third test image**Prediction of mask 3**

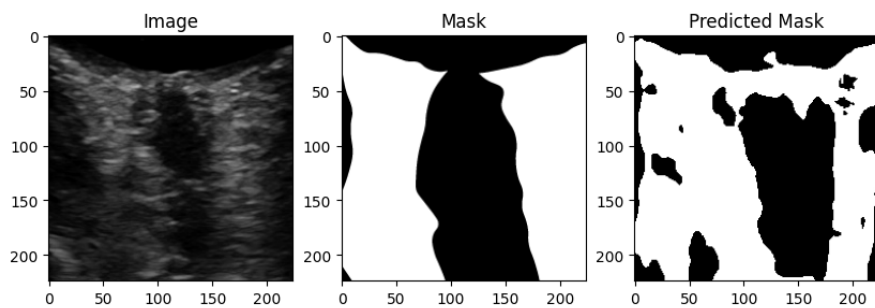


**FIGURE 39 –** Mask 3 of the first test image

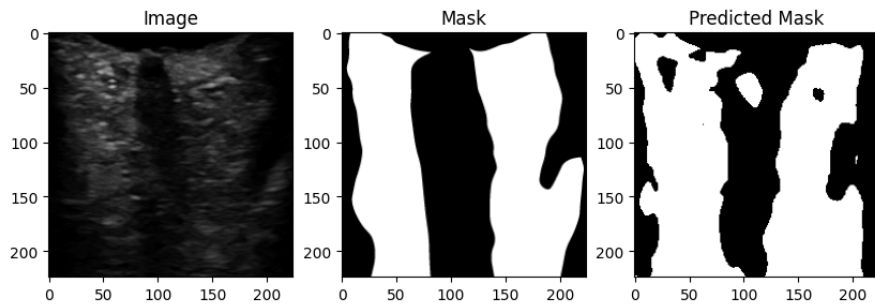


**FIGURE 40 –** Mask 3 of the second test image

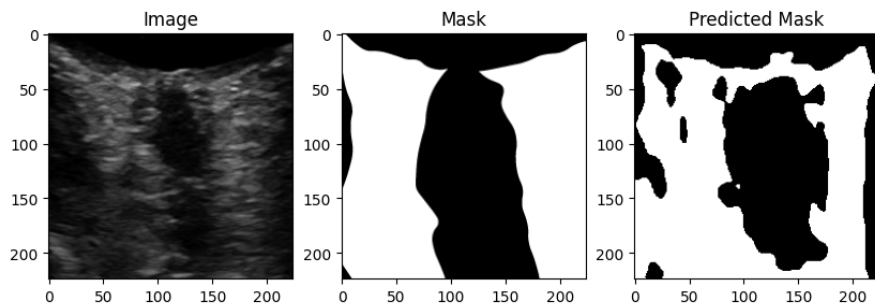


**FIGURE 41 –** Mask 3 of the third test image

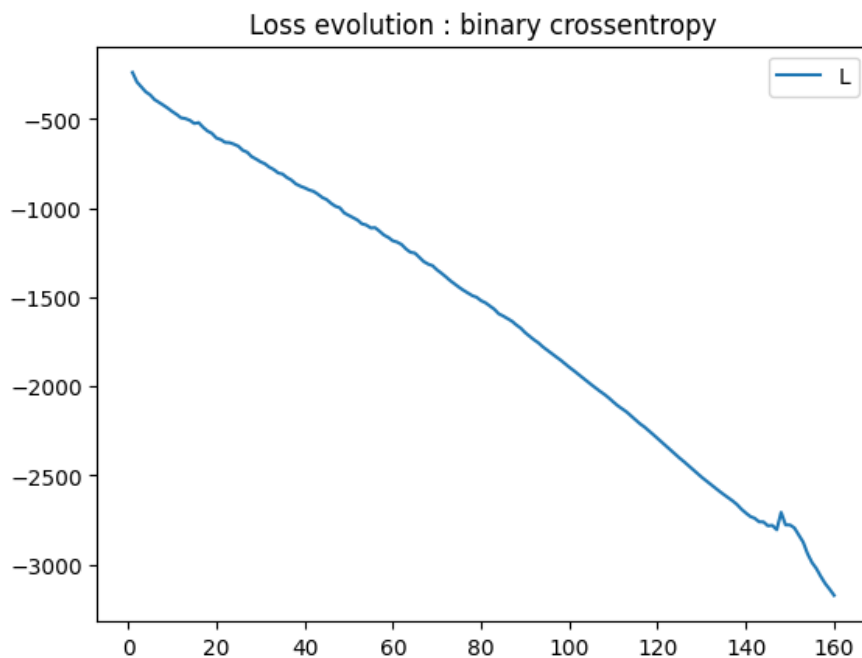
#### 6.4.3 Performance evaluation and metrics

For mask 1 :

**TABLE 1 – Metrics quantities of mask 1**

	Dice Coefficient	Pixel Accuracy	IoU
Image 1	0.67	0.57	0.508
Image 2	0.64	0.54	0.47
Image 3	0.76	0.64	0.62

And then here's the evolution of the loss, through epochs :

**FIGURE 42 – Loss evolution for mask 1**

**For mask 2 :**

**TABLE 2 – Metrics quantities of mask 2**

	Dice Coefficient	Pixel Accuracy	IoU
Image 1	0.73	0.47	0.58
Image 2	0.83	0.54	0.71
Image 3	0.76	0.64	0.62

And then here's the evolution of the loss, through epochs :

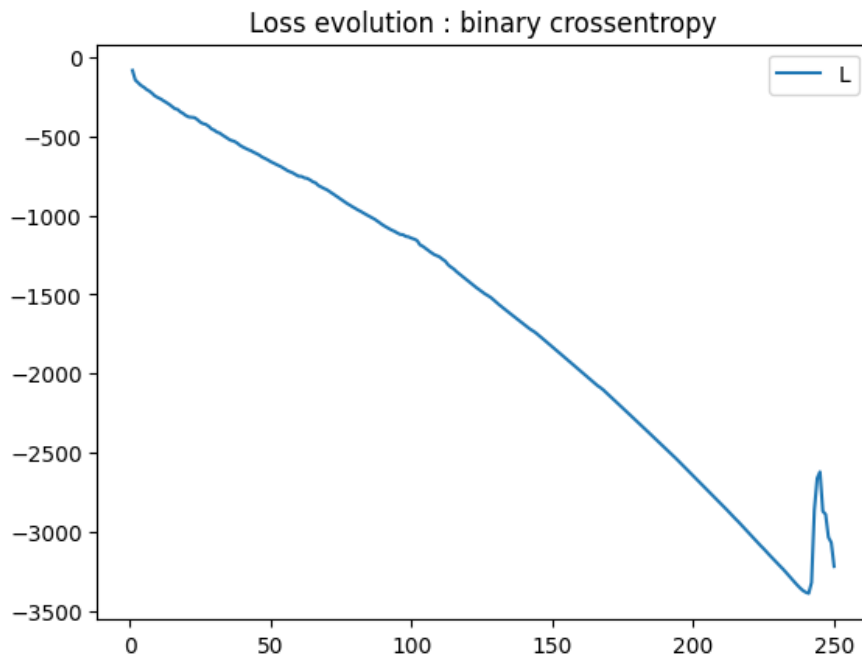


**FIGURE 43 –** Loss evolution for mask 2

**For mask 3 :**

**TABLE 3 –** Metrics quantities of mask 3

	Dice Coefficient	Pixel Accuracy	IoU
Image 1	0.77	0.33	0.63
Image 2	0.83	0.36	0.71
Image 3	0.7	0.33	0.54

And then here's the evolution of the loss, through epochs :

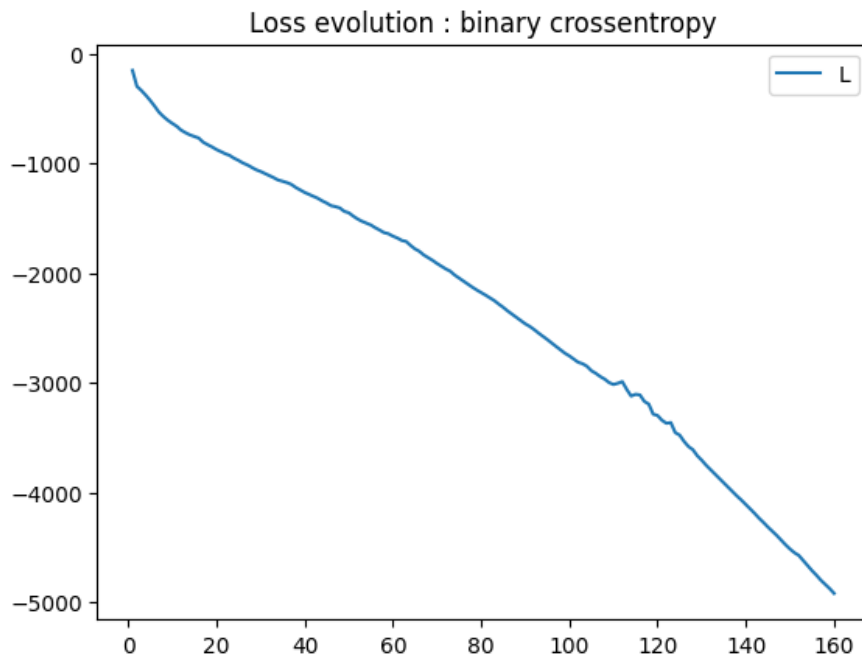


**FIGURE 44 –** Loss evolution for mask 3

#### 6.4.4 Conclusion

The application of transfer learning allowed us to improve the segmentation performance compared to training from scratch with only 12 images. By leveraging the knowledge acquired from the pretrained encoder, the model could effectively extract meaningful features and capture intricate details within the ultrasound images. This resulted in more accurate and robust segmentation results, leading to better identification of different clusters or regions of interest.

Overall, transfer learning proved to be an effective strategy for enhancing the performance of our segmentation model in the context of limited training data. It allowed us to leverage the power of pretrained models and benefit from their learned representations, ultimately improving the quality of our segmentation results.

## 6.5 Alternative transfer learning approach

### 6.5.1 Description of the method

In this section, we explore an alternative transfer learning/fine-tuning approach to semantic segmentation, complementing the findings presented in the existing chapter on transfer learning. Different architectures such as a custom U-net with variable depth of the VGG and ResNet-based encoder as well as multiple other networks provided by the library "segmentation-models" have been tested. This approach relied on the frozen imagenet-pretrained encoder backbone, further training of the decoder with other medical image data and finally retraining last layers of the network on our specific dataset.

Different data augmentations such as horizontal flipping and random cropping were utilized to increase the volume of the training data.

As an additional experiment we've tried to perform a primitive ensembling of multiple networks (weighted sum of their predictions) or segmentation with traditional clustering approaches such as Gaussian mixture models or K-means applied on the feature map of the penultimate layer of the network. Ensembling enables regulation of the width of the predicted sheath by picking a threshold (from 1 up to the number of networks in ensemble) from which a pixel should be identified as background and also opens possibilities for trying out further classification techniques on its output.

### 6.5.2 Results

**Prediction of mask 2 (purple) overlayed with the ground truth (yellow)**

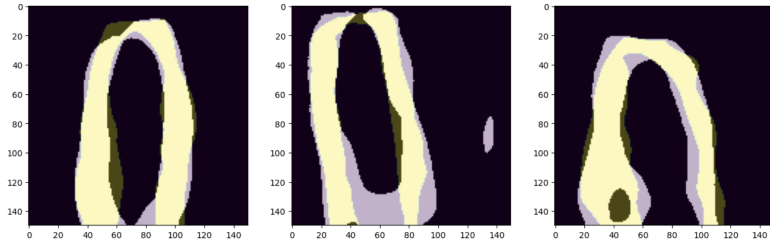


**FIGURE 45 –** Results of the custom U-net on the test set, 73% IOU

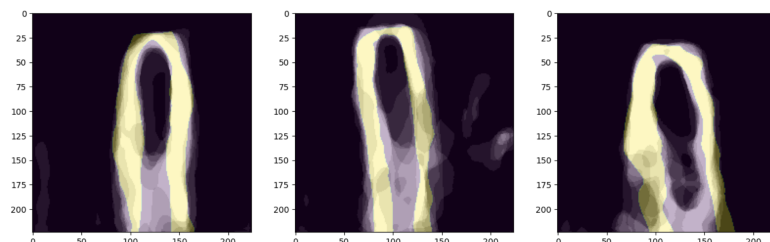


**FIGURE 46 –** Results of ensemble of networks

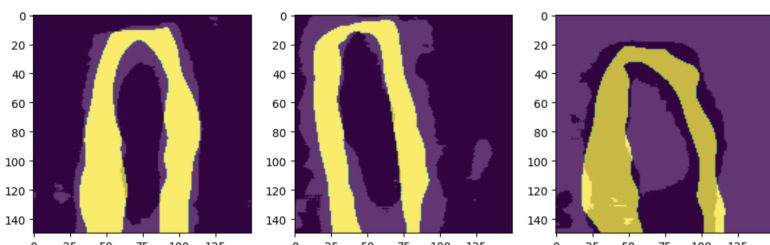


**FIGURE 47 –** Results of the GMM on the penultimate layer features

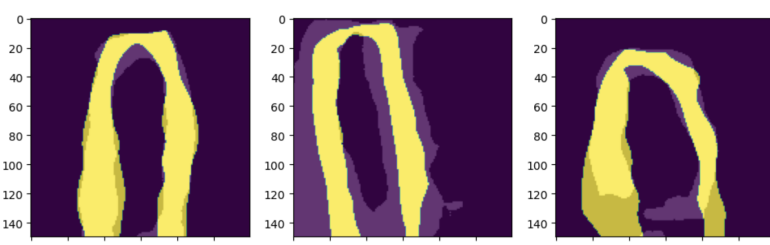


**FIGURE 48 –** Results of K-means on the penultimate layer features

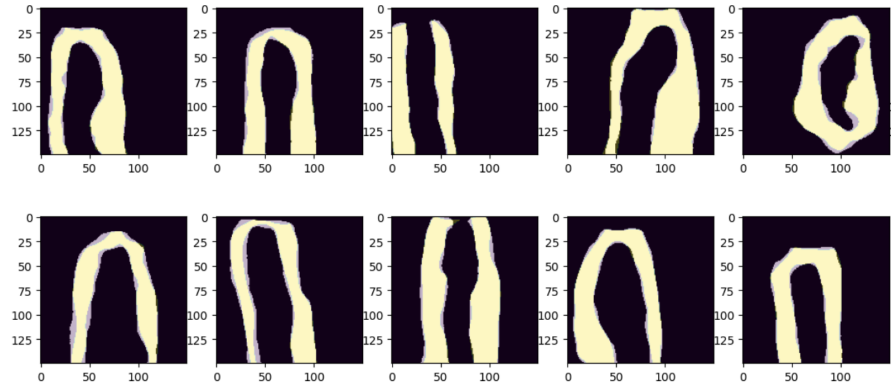


**FIGURE 49 –** Results on the training data

#### Segmentation based on 4-classes ground truth images

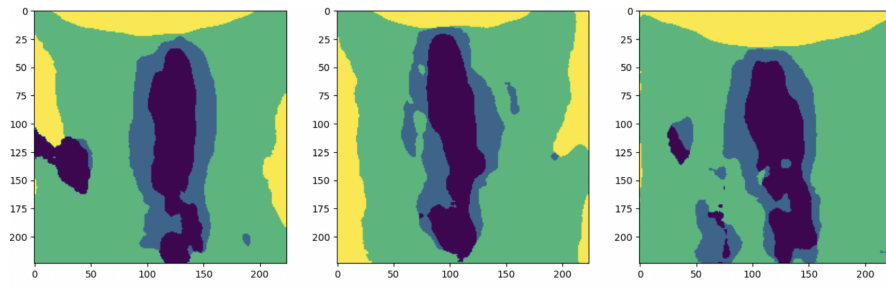


**FIGURE 50 –** Results of the U-net, mean IOU 65% for the sheath, 79% overall

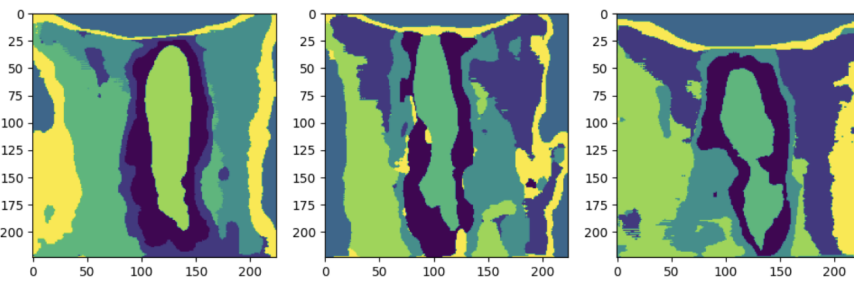


**FIGURE 51 –** GMM with 7 clusters on U-net's penultimate layer feature map

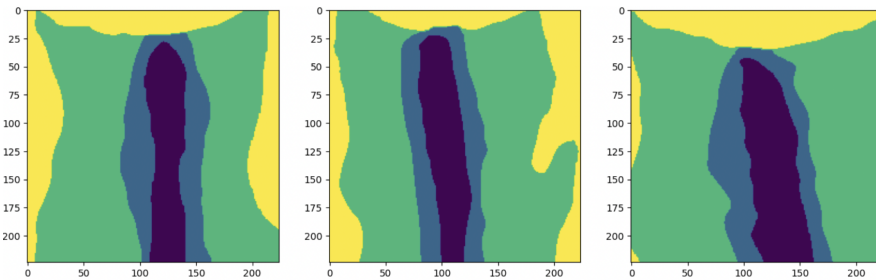


**FIGURE 52 –** ground truth testing annotations

### 6.5.3 Performance evaluation and metrics

The loss function employed was weighted cross-entropy which allowed to draw model's attention to the imbalance of classes. IOU was chosen as the main evaluation metric.

#### Example of dynamics of loss and IOU progressions with training

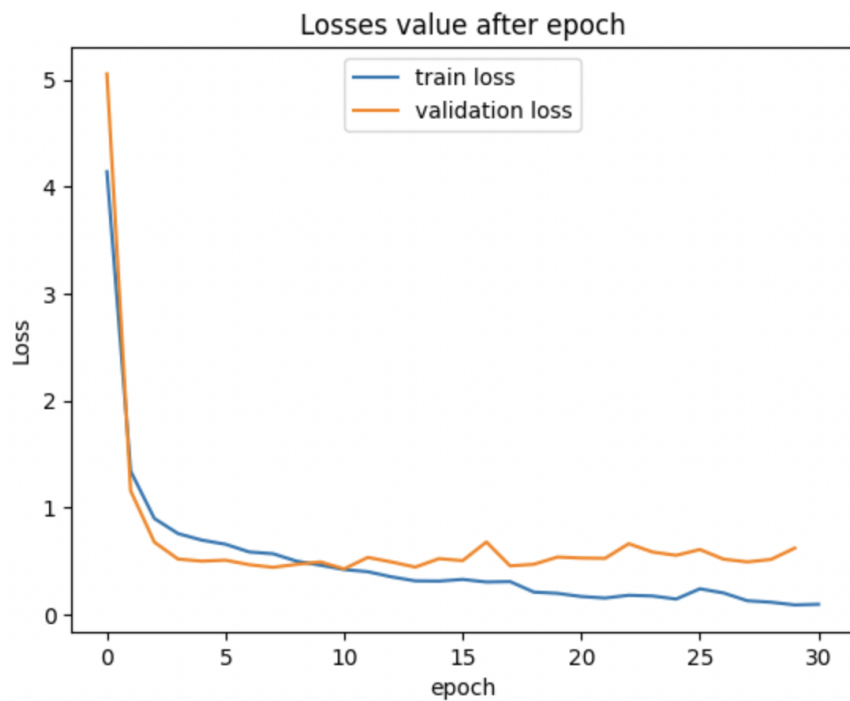


**FIGURE 53 –** loss decrease during the first 10 epochs

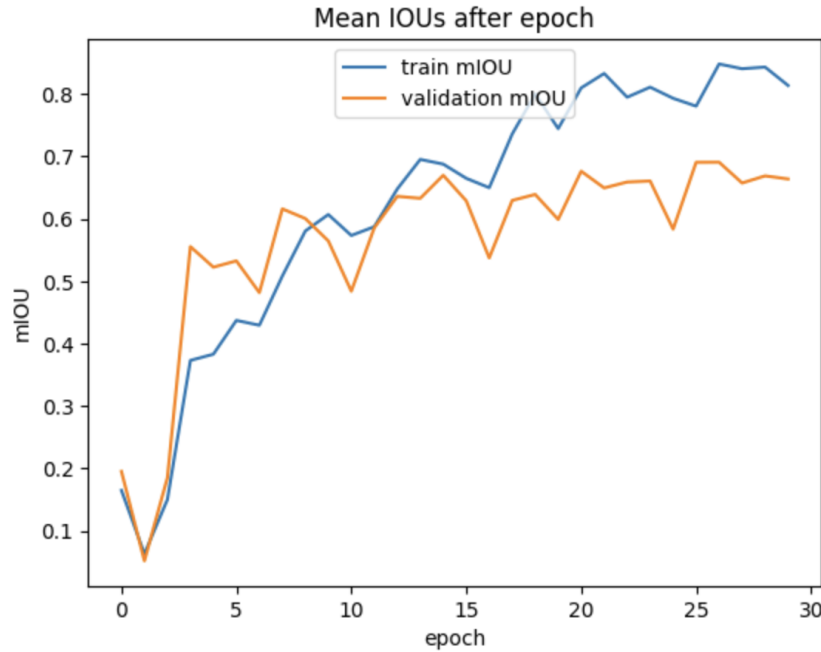


**FIGURE 54 –** IOU improvement during the first 10 epochs

The best acquired mean IOU on the test set was about 73%. It's worth noting that this result applies to the center-top cropped images as you may see it in figure 42. We consider this little "hack" in metric evaluation valid since we are only interested in the measurement of the width of the sheath in the beginning of the nerve. On the training set after several epochs it starts to oscillate around 88-92%. It's also worth noting that 73% is the value of IOU only on the class of interest. Together with the background it may jump up to 80%.

#### 6.5.4 Conclusion

Although a mean IOU of 73% may not appear substantial at first glance, we can see that the model tends to identify the sheath region as wider than it is in the ground truth mask, particularly in the case of GMM. While this outcome may not provide precise measurements of the sheath diameter, we believe that it can serve as an upper bound estimator for this task. By adjusting the training process's loss function to assign greater weight to the sheath and less weight to the background, it should be feasible to obtain an even more resilient upper bound.

## 7 Conclusion

In this project, we focused on ultrasound image segmentation of the optic nerve sheath to measure its diameter. We explored various methods, including feature extraction using the VGG Model, clustering algorithms, and image processing techniques, but none of them provided satisfactory accuracy.

To address this, we adopted the Unet model and trained it on our initial dataset. Despite the limited data, the results improved when we applied data augmentation techniques such as flipping and rotating. However, the breakthrough came when we incorporated transfer learning by training the encoder part of the Unet model on a large dataset for breast cancer detection and the decoder parts on our initial dataset. This transfer learning approach significantly enhanced the model's performance.

Furthermore, we utilized another large dataset specifically focused on optic nerve sheath images and applied transfer learning once again. This final step yielded the best results of the entire project, highlighting the effectiveness of leveraging external <https://www.overleaf.com/project/645c9d6b0d3636f5b6936f6ddatasets>.

The primary challenges we encountered throughout the project were attributed to the limited availability of data. Despite these limitations, we were able to make significant progress by employing state-of-the-art techniques and incorporating transfer learning.

Overall, our project demonstrated the potential of ultrasound image segmentation and the Unet model in accurately measuring the diameter of the optic nerve sheath. Future research should focus on acquiring larger datasets for improved model training and further exploring the potential of transfer learning in similar medical image analysis tasks.

## 8 Future Directions and Perspectives

While the most obvious next step is evaluating the model's performance on a larger dataset, we believe there are ways to improve the quality of segmentation using currently available resources. For example, applying an SVM/Random Forest/XGBoost to the penultimate layer feature map of U-net, exploring other approaches to the ensembling of networks from "segmentation-models" library, pretraining those networks on different medical image data, trying different modifications of U-net such as adding recurrent blocks or exploiting attention mechanism.

## 9 Bibliography

- **Deep Learning in Medical Ultrasound Analysis : A Review** By : Sheng-feng Liu , Yi Wang , Xin Yang , Baiying Lei , Li Liu , Shawn Xiang Li , Dong Ni , Tianfu Wang.
- **Automatic segmentation of the optic nerve in transorbital ultrasound images using a deep learning approach** By : Kristen M. Meiburger , Andrea Naldi, Piergiorgio Lochner, Francesco Marzola.
- **Optic Nerve Sheath Diameter Used as Ultrasonographic Assessment of the Incidence of Raised Intracranial Pressure in Preeclampsia** By : Clément Dubost, M.D., Agnès Le Gouez, M.D., Viridiana Jouffroy, M.D., Sandrine Roger-Christoph, M.D., Dan Benhamou, M.D., Frédéric J. Mercier, M.D., Ph.D., Thomas Geeraerts, M.D., Ph.D.
- **Breast cancer dataset** : <https://www.kaggle.com/datasets/aryashah2k/breast-ultrasound-images-dataset>
- **Optic nerve dataset** : <https://e-space.mmu.ac.uk/624643/>